

# The Unusual X-ray Spectrum of FU Orionis

Stephen L. Skinner

*CASA, Univ. of Colorado, Boulder, CO 80309-0389*

Kevin R. Briggs and Manuel Güdel

*Paul Scherrer Institute, Würenlingen and Villigen, CH-5235 Switzerland*

## ABSTRACT

FU Orionis objects (FUors) have undergone strong optical outbursts and are thought to be young low-mass stars accreting at high rates of up to  $\dot{M}_{acc} \sim 10^{-4} M_{\odot} \text{ yr}^{-1}$ . FUors have been extensively studied at optical and infrared wavelengths, but little is known about their X-ray properties. We have thus initiated a program aimed at searching for and characterizing their X-ray emission. First results are presented here for the prototype star FU Orionis based on observations obtained with *XMM-Newton*. Its CCD X-ray spectrum is unusual compared to those of accreting classical T Tauri stars (cTTS). The cool and hot plasma components typically detected in cTTS are present but are seen through different absorption column densities. The absorption of the cool component is consistent with  $A_V \approx 2.4$  mag anticipated from optical studies but the absorption of the hot component is at least ten times larger. The origin of the excess absorption is uncertain but cold accreting gas or a strong near-neutral wind are likely candidates. The hot plasma component accounts for most of the observed X-ray flux and thermal models give very high temperatures  $kT \geq 5$  keV. The most prominent feature in the X-ray spectrum is an exceptionally strong Fe K emission line at 6.67 keV and weak emission from fluorescent Fe I at  $\approx 6.4$  keV may also be present. The high plasma temperature clearly demonstrates that the emission is dominated by magnetic processes. We discuss possible origins of the unusual X-ray spectrum in the context of a complex physical environment that likely includes disk accretion, a strong wind, magnetic activity, and close binarity.

*Subject headings:* stars: individual (FU Orionis) — stars: pre-main sequence — X-rays: stars

## 1. Introduction

FU Orionis objects (FUors) undergo some of the most extreme variability seen in low mass pre-main-sequence (PMS) stars. The classical FUors are characterized by optical outbursts during which the star increases in brightness by several magnitudes over  $\sim 1 - 10$  years and then slowly decays on timescales of  $\sim 20 - 100$  years. The underlying cause of these flare-ups is not known. Herbig (1977) considered several possible mechanisms but none emerged as a clear favorite. More recent work has focused on the idea that the brightenings are due to a dramatic increase in the accretion rate through a circumstellar disk, perhaps triggered by disk instabilities or interactions with a close binary companion. A review of the FU Orionis phenomenon and the evidence favoring episodic accretion as its cause was given by Hartmann & Kenyon (1996 = HK96). Potential difficulties with the accretion interpretation have been discussed by Petrov & Herbig (1992).

The sample of classical FUors for which optical outbursts have actually been observed is small. These include FU Ori itself, as well as V1057 Cyg, V1515 Cyg, and V1735 Cyg. Because of their unusual variability, the classical FUors have been extensively studied at optical, infrared, and submillimeter wavelengths. Their properties are summarized by Herbig (1966, 1977), HK96, and Sandell & Weintraub (2001). However, there have been no previous X-ray observations targeted specifically at classical FUors, and their X-ray properties are largely unknown. We have thus initiated a program aimed at searching for and characterizing their X-ray emission. We would like to know if the X-ray spectra of FUors are similar to classical T Tauri stars (cTTS). Both FUors and cTTS are accreting low-mass PMS stars, and the FUor V1057 Cyg was a T Tauri star before erupting in 1969 (Herbig 1977). It is thus believed that FU Ori-like outbursts represent a transient (and possibly recurrent) phase in the life of a T Tauri star.

We present here first results from X-ray observations of the prototype FU Orionis. It brightened optically by about 6 magnitudes during 1936 - 1937 (Herbig 1966) and is still in slow decline. It has an optical spectrum and colors resembling an F-G supergiant, a near-IR excess, a high Li abundance, and strong P Cygni optical and UV line profiles indicative of mass loss, but no bipolar CO outflow or HH objects have been detected (HK96). Features associated with an expanding circumstellar shell are seen in the spectra (Herbig 1966). A near-IR companion is present at an offset of  $0.50''$  (230 AU at  $d = 460$  pc) and  $PA = 161^\circ$  (Wang et al. 2004). This object is about 4 mag fainter at K band than FU Ori and has a near-IR excess, so is likely a PMS star (Reipurth & Aspin 2004). Interferometry observations at H and K probe the star on AU distance scales, showing evidence for an accretion disk with  $\dot{M}_{acc} \approx 10^{-4} M_\odot \text{ yr}^{-1}$  and a mysterious hot spot located at a projected separation of 10 AU (Malbet et al. 2005). The physical origin of the hot spot is uncertain,

but Malbet et al. argue that it may be the signature of a very close companion. If so, this would make FU Ori a triple system.

We find that the X-ray spectrum of FU Ori is quite unusual compared to what is typically observed in cTTS. The spectrum does show the cool and hot components usually seen in cTTS, but the components are viewed through different absorption columns. We discuss possible interpretations of the unusual spectrum and note qualitative similarities with the jet-driving T Tauri star DG Tau A.

## 2. XMM-Newton Observations

A short 16 ksec *XMM-Newton* observation of FU Ori was obtained on 8 March 2004. FU Ori was clearly detected but the observation was adversely affected by high background radiation (Skinner et al. 2005).

We present here the results from a longer follow-up observation which began on 2005 April 3 at 15:36 UT and ended at 02:37 UT on April 4. Data were acquired with the European Photon Imaging Camera (EPIC), which provides CCD imaging spectroscopy from the PN camera (Strüder et al. 2001) and two nearly identical MOS cameras (MOS1 and MOS2; Turner et al. 2001). The observation was obtained in full-window mode using the medium optical blocking filter. The EPIC cameras provide energy coverage in the range  $E \approx 0.2 - 15$  keV with energy resolution  $E/\Delta E \approx 20 - 50$ . The MOS cameras provide the best on-axis angular resolution with FWHM  $\approx 4.3''$  at 1.5 keV.

Data were reduced using the *XMM-Newton* Science Analysis System (SAS vers. 6.1). Event files generated during the standard processing were filtered to select good event patterns. Time filters were applied to remove segments of high background exposure. This yielded 26.9 ksec of low-background PN exposure (including 20.9 ksec of contiguous data in the last half of the observation) and 32.2 ksec of contiguous exposure per MOS. Spectra and light curves were extracted from a circular region of radius  $R_e = 15''$  centered on FU Ori, corresponding to  $\approx 68\%$  encircled energy at 1.5 keV. Background spectra and light curves were obtained from circular source-free regions near the source (on the same CCD) and were compared with background extracted from an annular region around the source. The derived results were not significantly affected by the region used to extract background. The mean PN background rate in the vicinity of FU Ori measured during the usable periods of low-background exposure was  $1.09 \times 10^{-6}$  c s $^{-1}$  arcsec $^{-2}$  (0.5 - 7 keV). The SAS tasks *rmfgen* and *arfgen* were used to generate source-specific response matrix files (RMFs) and auxiliary response files (ARFs) for spectral analysis. The data were analyzed using the *XANADU*

software package <sup>1</sup>, including *XSPEC* vers. 12.2.0.

### 3. Results

#### 3.1. Spatial and Temporal X-ray Properties

Figure 1 shows the combined MOS 1 + MOS 2 image of FU Ori in the 0.5 - 7 keV band. The pipeline processing detected this source at position (J2000.) RA = 05h 45m 22.43s, Decl. = +09° 04' 12.2'', with a formal positional uncertainty of 0.30''. This position is offset 1.06'' from the *2MASS* position of FU Ori (2MASS J054522.3+090412; J = 6.52, H = 5.70, K = 5.16) and 1.04'' from the *HST* Guide Star Catalog (GSC) position. Our own image analysis using data from all three EPIC detectors gives an X-ray position nearly identical to that determined by the pipeline processing but with slightly smaller offsets of 1.04'' from *2MASS* and 0.95'' from *HST* GSC. These  $\approx 1''$  offsets are within the positional accuracy expected for *XMM* EPIC at the signal-to-noise ratio of our data. We find no other objects within 15'' of FU Ori in the HST GSC 2.2, USNO B1.1 or 2MASS data bases. Thus, the X-ray emission most likely originates in FU Ori but a contribution from the faint IR companion located 0.5'' to the south is not ruled out since *XMM-Newton* cannot spatially resolve the two.

Since the X-ray spectrum shows both cool and hot plasma components (Sec. 3.2), we have measured the X-ray centroid positions in the combined MOS 1 + MOS 2 image in the soft 0.5 - 2 keV and harder 2 - 7 keV bands. These measurements indicate that any offset between the soft and hard band positions is no larger than  $\approx 0.95''$ , which is slightly less than the 1.1'' MOS pixel size. Higher angular resolution observations will be needed to determine if a sub-arcsecond offset is actually present.

No large-amplitude flares are visible in the X-ray light curves. The last 20.9 ksec of contiguous low-background PN exposure gives a mean background-subtracted PN count rate of 7.2 c ksec<sup>-1</sup> (0.5 - 7 keV;  $R_e = 15''$ ). A  $\chi^2$  variability test on this 20.9 ksec segment binned at 2000 s intervals yields a probability of constant count rate  $P_{const} = 0.52$  ( $\chi^2/\text{dof} = 8.1/9$ ). The MOS detectors are less affected by background flares and thus provide more usable exposure than the PN, but at lower count rates. The summed MOS1 + MOS2 light curve for the last 32.2 ksec of exposure has a mean background-subtracted rate of 4.9 c

---

<sup>1</sup>The *XANADU* X-ray analysis software package is developed and maintained by NASA's High Energy Astrophysics Science Archive Research Center. See <http://heasarc.gsfc.nasa.gov/docs/xanadu/xanadu.html> for further information.

$\text{ksec}^{-1}$  (0.5 - 7 keV;  $R_e = 15''$ ) and a  $\chi^2$  test gives  $P_{const} = 0.92$  ( $\chi^2/\text{dof} = 6.7/13$ ) using 2000 s bins.

Based on the above analysis, there is no compelling evidence for X-ray variability in FU Ori during the April 2005 observation. However, the EPIC PN fluxes of FU Ori in this observation were about 50% larger than in the shorter March 2004 observation, as determined by the pipeline processing and our spectral analysis. It thus seems likely that FU Ori did vary during the  $\approx 1$  year time interval between the two observations. Since the inferred variability is based on a comparison with high-background data acquired in March 2004, further time monitoring would be useful to confirm the variability and constrain its timescale.

### 3.2. The X-ray Spectrum of FU Ori

Figure 2 shows the PN spectrum of FU Ori. The spectrum reveals a cool component below  $\sim 2$  keV and a hotter component above  $\sim 2$  keV. Strong line emission from the Fe  $K\alpha$  complex near 6.7 keV is clearly present. We discuss spectral models and plasma properties below.

#### 3.2.1. Thermal Emission Models

Since cool and hot plasma are clearly present, we first attempted to fit the spectrum with a *single-absorption* two-temperature (2T) optically thin thermal plasma model. This model assumes that the emission is due to a multi-temperature plasma with a cool component at temperature  $kT_1$  and hotter component at  $kT_2$ , where both components are viewed through the same absorption column density  $N_H$ . We refer to this model in abbreviated notation as  $N_H \cdot (kT_1 + kT_2)$ . Spectral fits with this model can reproduce the hard part of the spectrum above  $\approx 2$  keV with a high-temperature plasma  $kT_2 \approx 7$  keV and strong absorption  $N_H \approx 8 \times 10^{22} \text{ cm}^{-2}$ . However, the overall fit is unacceptable (reduced  $\chi^2 > 1.5$ ) because the model flux is heavily attenuated below  $\approx 1$  keV for reasonable values  $kT_1 \leq 1$  keV. As a result, the model fails to account for the emergent flux below  $\approx 1$  keV that is clearly present in the observed spectrum. These results suggest that the cool plasma below  $\approx 1$  keV is viewed through lower absorption than that inferred above for the hot plasma.

The inability to reproduce the spectrum using a single-absorption 2T model is somewhat surprising because the X-ray spectra of most TTS can be reasonably well matched with this

type of model, including TTS in the Orion region (Getman et al. 2005). However, it has recently been noted that such a model could not reproduce the X-ray spectrum of the jet-driving TTS DG Tau A (Güdel et al. 2005). In that case, an acceptable fit was obtained by allowing the absorption column density for each plasma component to be different. We thus attempted to fit the spectrum of FU Ori using a *double-absorption* model of the form  $N_{H,1} \cdot kT_1 + N_{H,2} \cdot kT_2$ .

The double-absorption model yields very good results. Table 1 gives best-fit parameters for this model when all abundances are held fixed at solar values (Model A) referenced to Anders & Grevesse (1989), and for the case where the Fe abundances of both components are allowed to vary independently (Model B). The variable Fe abundance model shown in Figure 2 provides a slightly better fit than obtained with solar abundances, but this is accomplished by increasing the Fe abundance of the hot component to a value greater than solar in order to reproduce the strong Fe K line. Figure 3 compares the fits to the Fe K line obtained with solar abundances and an enhanced Fe abundance.

The temperature and absorption column density derived for the cool component from the above double-absorption models are quite reasonable. The temperature  $kT_1 \approx 0.7$  keV ( $\approx 8$  MK) is typical of cool plasma detected in most TTS in Orion (Preibisch & Feigelson 2005). Furthermore, the corresponding best-fit absorption from models A and B is in the range  $N_{H,1} \approx (4.2 - 5.5) \times 10^{21} \text{ cm}^{-2}$ , but with rather large uncertainties (Table 1). The best-fit values equate to an extinction  $A_V \approx 1.9 - 2.5$  mag using the  $N_H$  to  $A_V$  conversion given by Gorenstein (1975). These values are in good agreement with that determined from the color excess  $E(B - V) = 0.8$  for FU Ori (Herbig 1977) and with the values  $A_V = 2.4$  mag (Adams, Lada, & Shu 1987) and  $A_V = 1.85$  mag (Kenyon, Hartmann, & Hewett 1988) derived from fits of its spectral energy distribution. It thus seems very likely that we are detecting cool X-ray emission that originates in FU Ori and is moderately absorbed by the same material that is responsible for the optical extinction.

The temperature inferred for the hot component in the above double-absorption models is  $kT_2 \approx 5.6 - 7.2$  keV (65 - 83 MK; Table 1). These temperatures are high but nevertheless within the range observed for magnetically-active TTS in Orion (Preibisch & Feigelson 2005). However, the absorption inferred for this hot component is much larger than anticipated from optical extinction estimates. The X-ray spectral fits from Models A and B give  $N_{H,2} \approx (8.4 - 12.8) \times 10^{22} \text{ cm}^{-2}$ , which corresponds to  $A_V \approx 38 - 58$  mag using Gorenstein (1975). The nature and location of the material responsible for the strong X-ray absorption are uncertain, but the apparent absence of such high absorption at visible wavelengths suggests that it is primarily gaseous.

Although the above double-absorption model provides an acceptable fit to the spectrum,

it may be overly simplistic in one respect. It assumes that the plasma viewed through low absorption is isothermal ( $kT_1$ ), and likewise for that viewed through high absorption ( $kT_2$ ). If the low or high absorption components (or both) originate in a multi-temperature corona, then it would be more physically realistic to replace  $kT_1$  with a multi-temperature plasma, and likewise for  $kT_2$ . We return to this issue in Section 4.3.

### 3.2.2. Fe Emission Lines

The spectrum between 6 - 7 keV is dominated by strong Fe line emission. The best-fit line centroid energy in the PN spectrum is  $E_{line} = 6.68$  [6.56 - 6.75; 90% conf.] keV, which is identified with the Fe K shell complex including Fe XXV. This line emits maximum power at  $T_{max} \approx 10^{7.6}$  K, providing unambiguous evidence for hot plasma. The Fe K line flux accounts for about one-fourth of the observed flux in the 0.5 - 7 keV band (Table 1). A weak feature is also seen near  $E \approx 7.79$  keV as a  $2\sigma$  excess in one bin (Fig. 2). The feature is of low significance but if it is weak line emission the most likely candidate would be Ni XXVII at lab energy  $E_{lab} = 7.806$  keV. A broad emission peak is also present near 0.8 - 1.1 keV. Numerous Fe and Ne lines and the O VIII Ly $\beta$  line occupy this portion of the spectrum but these lines are not resolved at EPIC’s spectral resolution.

The value of the Fe abundance for the cool component ( $Fe_1$ ) determined from the variable abundance model is quite uncertain but does converge to values at or slightly below solar (Model B in Table 1). As mentioned above, this model requires a high Fe abundance for the hot component ( $Fe_2$ ) in order to accommodate the strong Fe K line. The best-fit  $Fe_2$  abundance depends somewhat on the amount of spectral binning used and we obtain values in the range  $Fe_2 = 2.20 - 2.78 \times \text{solar}$  (Table 1 Notes). But, 90% confidence intervals do allow a value that is barely consistent with solar. These variable Fe abundance fits constrain the width of the Fe K line to its instrumentally-broadened value, but no significant differences in the  $Fe_2$  abundance are found if the line width is allowed to vary.

If the global metallicity  $Z$  is allowed to vary instead of just Fe, then the derived absorption and temperatures are nearly identical to those of Model B (Table 1 Notes). The metallicity of the hot component is largely determined by the Fe K line and likewise converges to a value above solar, but is barely consistent with solar at the lower 90% confidence bound.

A weak excess above the continuum is present at 6.36 [6.30 - 6.42] keV, as can be seen in Figure 3. This excess may be due to weak fluorescent Fe I emission that would most likely originate in cool neutral material being illuminated by the high-temperature X-ray source.

If an additional Gaussian component at 6.36 keV is added to the thermal models in Table 1, a slight improvement in the fit is obtained and the reduced  $\chi^2$  values decrease by 5% - 10%. Adding the 6.36 keV Gaussian line does not significantly affect the best-fit Fe abundance of the hot component in the thermal models.

In summary, the X-ray spectra do not place a definitive constraint on the Fe abundance of the cool plasma component. But if the emission is due to an optically thin plasma then the Fe abundance of the hot component must be near-solar to account for the exceptionally strong Fe K line. It seems quite unlikely that the Fe abundance of the hot component in the FU Ori spectrum is strongly depleted relative to the solar photospheric value, as has been found for some accreting T Tauri stars (Kastner et al. 2002; Schmitt et al. 2005). In a more general context, previous studies of active late-type stars indicate that the coronal Fe abundance is depleted relative to the solar photospheric value in some stars but not in others (reviewed by Güdel 2004).

### 3.2.3. A Power-law Continuum?

Because of the unusually hard continuum that is clearly present above 2 keV, we have also attempted to fit the spectrum using a hybrid model consisting of a cool lightly-absorbed optically thin thermal plasma plus a heavily-absorbed power-law continuum and a Gaussian Fe K line. The results of this model are given in Table 1 as Model D with components  $N_{H,1} \cdot kT_1 + N_{H,2} \cdot (PL + GAUS)$ .

Interestingly, this hybrid model yields a better fit than that obtained above with two thermal components as measured by a reduced  $\chi^2$  that is  $\approx 35\%$  smaller. As Figure 4 shows, much of this improvement comes from a tighter fit to the continuum above  $\approx 2$  keV. There is very little change in the parameters derived for the cool plasma, but the inferred absorption for the hot plasma  $N_{H,2}$  is about a factor of two below that determined from the purely thermal models. Even so,  $N_{H,2}$  is still an order of magnitude larger than expected for FU Ori based on previously published  $A_V$  estimates.

The width of the Gaussian Fe K line profile was allowed to vary in this hybrid model. When the PN spectrum is binned to a minimum of 10 counts per bin the best-fit line width  $FWHM = 2.35 \sigma_{line} = 235$  eV (Table 1) is slightly broader than the value  $FWHM \approx 160$  eV expected for an instrumentally-broadened line at 6.7 keV, but the 90% confidence range is consistent with no excess broadening. This fit attempts to account for some of the excess near 6.4 keV by broadening the Fe K line (Fig. 4 inset) and thus overestimates the true line width. If a second Gaussian component is added to model the weak excess near 6.4 keV then



the best-fit Fe K line width is reduced to  $\text{FWHM} = 148 \text{ eV}$ , consistent with an unbroadened line. Thus, we find no strong evidence for non-instrumental broadening at Fe K but higher energy resolution is needed to obtain a definitive line width measurement.

Thus, from the standpoint of goodness-of-fit, the hybrid thermal + power-law model (Model D) offers an improvement over the purely thermal models (Models A and B). However, either modeling strategy provides a statistically acceptable fit. A purely thermal model is more straightforward to interpret on physical grounds but we do comment further on the possibility of nonthermal emission in Section 4.5.

## 4. Discussion

### 4.1. Origin of the X-ray Emission

It is well-known that the optical spectrum of FU Ori shows complex two-component structure that cannot be matched by the spectrum of a normal star (Herbig 1966). We have found that its X-ray spectrum is also complex, consisting of cool and hot plasma components viewed through different absorption columns. We discuss possible interpretations below. The cool component could be coronal or shock-related, but the high temperature  $T_2 \approx 65 - 83 \text{ MK}$  determined from thermal fits of the hot component clearly points to a magnetic origin.

### 4.2. The Cool X-ray Component: Corona versus Shocks

The presence of a cool X-ray component viewed through an absorption column that is consistent with  $E(B-V)$  estimates is not surprising. The inferred temperature  $kT_1 \approx 0.7 \text{ keV}$  ( $T_1 \approx 8 \text{ MK}$ ) is very much in line with the cool X-ray emission detected in most TTS. The ubiquity and stable temperature of this component in a large sample of Orion TTS were noted by Preibisch & Feigelson (2005). This cool component is even present in active late-type coronal sources that are not accreting PMS stars, and thus likely reflects underlying conditions in the magnetic corona.

Some ambiguity arises in the above interpretation because cool high-density plasma in an accretion shock could masquerade as cool coronal emission in accreting PMS stars such as FU Ori. Higher energy resolution X-ray spectra are needed to obtain electron density estimates that can in principle be used to distinguish between high-density plasma in an

accretion shock and lower density coronal plasma. However, the interpretation of X-ray emission line density diagnostics is not straightforward because ultraviolet radiation from the accretion shock can alter X-ray line flux ratios, thus mimicking high densities. In addition, it has recently been argued that soft accretion shock X-rays may not be detectable in sources accreting at rates  $\dot{M}_{acc} \geq 10^{-9} \text{ yr}^{-1}$  because the shock is buried too deeply in the star's atmosphere (Drake 2005). The accretion rate of FU Ori is thought to be several orders of magnitude above this limit (Malbet et al. 2005), and the ability to detect accretion-induced X-rays in FU Ori is thus questionable. Finally we note that even though the temperature of the cool X-ray component determined from spectral fits has rather large uncertainties, the best-fit value  $kT_1 \approx 0.7 \text{ keV}$  is about twice as high as predicted from canonical accretion shock models using infall speeds of a few hundred  $\text{km s}^{-1}$  (Ulrich 1976).

Another possibility is that the cool X-ray component originates in a shocked jet or outflow at some distance from the star. This interpretation was put forward to explain the soft X-ray emission of DG Tau A (Güdel et al. 2005), which is known to drive a jet. However, no jet or strong collimated outflow has so far been found for FU Ori. But, FU Ori does have a strong wind and the wind speed inferred from its broad blueshifted  $H\alpha$  absorption feature is  $v_\infty \approx 250 - 400 \text{ km s}^{-1}$  (Croswell et al. 1987). If one assumes that a jet is present (but as yet undetected) at similar outflow speeds  $v \approx v_\infty$ , then the expected X-ray temperature for shocked jet emission is (Raga et al. 2002; Güdel et al. 2005):  $T_s = 1.5 \times 10^5 (v/100 \text{ km s}^{-1})^2 \text{ K} \approx 0.94 - 2.4 \text{ MK}$ , or  $kT \approx 0.08 - 0.21 \text{ keV}$ . These shock temperatures are a factor of  $\sim 3 - 8$  lower than the best-fit values for the cool component  $kT_1$  given in Table 1, but are barely consistent with the lower 90% confidence bound on  $kT_1$ .

Given the above considerations, we find no strong reason at present to favor an accretion shock or shocked outflow interpretation for the cool X-ray emission of FU Ori over the more conventional coronal interpretation. If higher resolution X-ray spectra and images are eventually obtained, the possibility of shock emission would be worth reconsidering.

### 4.3. On the Possibility of Inhomogeneous Absorption

It is apparent from the spectral fits discussed above that the X-ray absorption toward FU Ori is more complex than normally encountered in T Tauri stars and a physical interpretation must account for two absorption components. More than one interpretation is possible because of the limited X-ray spatial resolution. Since FU Ori is a known multiple system (Sec. 1) it may be that more than one star is contributing to the observed X-ray emission. Another possibility is that we are detecting X-ray emission from a multi-temperature plasma (such as a corona) viewed through inhomogeneous absorption. Evidence for patchy absorption

toward FU Ori has previously been mentioned by Adams, Lada, & Shu (1987).

To explore the coronal interpretation, we assume that the intrinsic X-ray emission arises in a multi-temperature corona with an admixture of cool ( $kT_1$ ) and hot ( $kT_2$ ) plasma, as is commonly the case in magnetically active PMS stars. Since FU Ori is accreting and is surrounded by a disk viewed at an inclination angle  $i \approx 55^\circ$  (Malbet et al. 2005), some of the coronal emission may be obscured by material close to the star. This could be the disk or cold gas in the accretion stream. However, at  $i \approx 55^\circ$  the entire corona would not necessarily be obscured. In particular, the polar region closest to the observer could incur very little disk obscuration, assuming a geometrically thin equatorial disk. And, if a bipolar outflow or jet is present (or has been in the past) then a low-density cavity might be evacuated near the poles (Clarke et al. 2005), allowing softer coronal photons to escape. However, coronal emission from subpolar latitudes could suffer heavy disk obscuration or strong absorption from cold accreting gas that impacts the star at subpolar latitudes.

We represent the above picture with a model of the form  $N_{H,1} \cdot (kT_1 + kT_2) + N_{H,2} \cdot (kT_1 + kT_2)$ . This model accounts for the multi-temperature structure that is expected for coronal plasma and assumes that a fraction of the coronal emission is viewed through relatively low absorption ( $N_{H,1}$ ) and the remainder through high absorption ( $N_{H,2}$ ).

The above model is referred to as Model C in Table 1. It has four normalization parameters. The low absorption component has a normalization parameter for the cool plasma  $\text{norm}_{1,cool}$  and for the hot plasma  $\text{norm}_{1,hot}$ . Likewise, the high-absorption component has norms  $\text{norm}_{2,cool}$  and  $\text{norm}_{2,hot}$ . When fitting the X-ray spectrum, all norms are allowed to vary independently except for  $\text{norm}_{2,cool}$  which is constrained to be  $\text{norm}_{2,cool} = [\text{norm}_{1,cool}/\text{norm}_{1,hot}] \times \text{norm}_{2,hot}$ . That is, we require the ratio of the norms, or equivalently, the emission measures, of the cool to hot plasma be the same in both the low and high absorption components. This would be expected if the emission seen through low and high absorption originates in the same structure (e.g. a multi-temperature corona). We choose to constrain  $\text{norm}_{2,cool}$  because this component is the least well-determined observationally. Almost all softer X-ray photons from the cool plasma component that pass through the high-absorption column will be absorbed and thus absent from the observed spectrum.

As the results in Table 1 show, Model C gives a slightly better fit to the PN spectrum than do Models A or B. Even so, there is very little change in the derived absorption, temperatures, and Fe abundance. The primary difference between Model C and Models A/B is in the underlying physical picture. Model C is based on the premise that the observed spectrum arises from viewing a single multi-temperature source through an inhomogeneous absorber. Thus, the emission detected through low absorption is an admixture of cool and hot plasma, as is that detected through high absorption. Another notable difference is

that the X-ray luminosity inferred from Model C is higher than that of the other models. Nevertheless, the value  $L_x = 1.7 \times 10^{31} \text{ ergs s}^{-1}$  (0.5 - 7 keV) from Model C is within the range observed for other low-mass PMS stars in Orion (Getman et al. 2005).

The relative contributions of cool and hot plasma to the total emission measure derived from Model C are somewhat uncertain, but the spectral fits suggest that they could be roughly equal. However, the total emission measure of the plasma viewed through high absorption is at least an order of magnitude larger than that detected through low absorption. Thus, if the emission does arise in a multi-temperature corona then the corona is almost totally obscured and only a small fraction of the softer coronal emission manages to escape. It is not yet clear what would create the escape path but clumpy absorption, scattering, or a low-density cavity evacuated by an existing or fossil jet or collimated outflow are possibilities.

The column density of the heavily-absorbed component determined from Model C is  $N_{\text{H},2} = 10.6 \times 10^{22} \text{ cm}^{-2}$ . This includes the small contribution  $N_{\text{H}} \approx 0.4 \times 10^{22} \text{ cm}^{-2}$  that is known to be present based on the optical extinction. The excess absorption of the hot component is then  $N_{\text{H},2}^{(excess)} = 10.2 \times 10^{22} \text{ cm}^{-2}$ . If the accretion column is responsible for this excess, then we can take the minimum inner disk radius  $r_{min} = 5.5 R_{\odot} = 3.8 \times 10^{11} \text{ cm}$  (Malbet et al. 2005) as the approximate length of the absorption column. Realistically, this value should be interpreted as an upper limit because viewing geometry considerations make it unlikely that we are looking through the entire length of the accretion column. Thus, if the strong absorption is due to accreting gas then the mean number density in the accretion column is  $n_{\text{H}} \geq 3 \times 10^{11} \text{ cm}^{-3}$ .

#### 4.3.1. Wind Absorption

In the above, it was assumed that the accretion flow is primarily responsible for the heavy X-ray absorption. However, the strong stellar wind of FU Ori may also contribute. Radiative transfer models that assume rapid wind acceleration give a high mass loss rate for FU Ori of  $\dot{M} \sim 10^{-5} M_{\odot} \text{ yr}^{-1}$  and P-Cygni type H $\alpha$  absorption features imply a terminal wind speed  $v_{\infty} \approx 250 - 400 \text{ km s}^{-1}$  (Croswell et al. 1987). There is some evidence that the wind arises from the surface of the accretion disk (Calvet, Hartmann, & Kenyon 1993).

A VLA radio observation did not detect FU Ori with a  $3\sigma$  upper limit on its 3.6 cm flux density  $S_{3.6} \leq 0.05 \text{ mJy}$  (Rodriguez, Hartmann, & Chavira 1990). Assuming a spherically-symmetric wind with temperature  $T_{wind} \approx 5000 \text{ K}$  (Croswell et al. 1987),  $v_{\infty} = 400 \text{ km s}^{-1}$ , and a distance of 460 pc, the radio non-detection gives an upper limit on the ionized mass-loss rate  $\dot{M}_{ion} \leq 4.4 \times 10^{-8} M_{\odot} \text{ yr}^{-1}$  (eq. [7] of Skinner, Brown, & Stewart 1993).

Thus, the high mass-loss rate derived by Crosswell et al. (1987) can only be reconciled with the radio data if the wind is largely neutral.

The predicted neutral hydrogen column density along the line-of-sight toward the star for a spherically-symmetric homogeneous wind with mass loss rate  $\dot{M} = 10^{-5} M_{\odot} \text{ yr}^{-1}$ , terminal speed  $v_{\infty} = 400 \text{ km s}^{-1}$ , and stellar radius  $R_{*} \approx 4 R_{\odot}$  (Calvet et al. 1993) is  $N_{\text{H,wind}} \sim 10^{24} \text{ cm}^{-2}$ . This is about ten times larger than that determined for the heavily-absorbed component in the X-ray spectrum. The X-ray data could be brought into agreement with the predicted  $N_{\text{H,wind}}$  if the mass-loss rate were about an order of magnitude smaller, that is  $\dot{M} \sim 10^{-6} M_{\odot} \text{ yr}^{-1}$ . The mass loss rate determined from radiative transfer models is known to be sensitive to the poorly-known wind temperature and wind velocity profile, and if the wind is slowly accelerated then lower mass loss rates are possible and  $\dot{M} \sim 10^{-6} M_{\odot} \text{ yr}^{-1}$  is not out of the question (Crosswell et al. 1987).

If the strong X-ray absorption is indeed due to FU Ori’s massive wind, then an additional question arises. Where does the cool component in the X-ray spectrum originate? If it is cool coronal emission that originates close to the star, then it must somehow escape through the wind without being totally absorbed. This would seemingly require either an inhomogeneous wind or a non-spherical wind geometry that allows some soft coronal photons to reach the observer. Here, it is worth mentioning that a slowly accelerating non-spherical collimated flow was mentioned by Crosswell et al. as a possible solution to matching the observed optical line properties of FU Ori, including the absence of redshifted emission. On the other hand, if the simplistic picture of a spherically-symmetric homogeneous wind is approximately correct then a calculation of the radius of X-ray optical depth unity in the wind shows that the cool X-ray emission must emerge far from the star.

#### 4.4. Issues Concerning Binarity

It may be that more than one X-ray source is contributing to the observed spectrum. This is conceivable since FU Ori is known to be a double or perhaps even a triple system. If each component has a disk and the disks are viewed at different inclination angles (or if one star is viewed through the disk of another), then multiple absorption components would be expected.

It seems unlikely that the hard heavily-absorbed X-ray component originates in the near-IR companion  $0.5''$  away if its extinction is only  $A_V \approx 1.1 \text{ mag}$  (Wang et al. 2004). The extinction toward the hard X-ray component is much higher (Sec. 3.2.1). Assuming that the extinction toward the near-IR companion has not been underestimated, we are left with

the intriguing possibility that the hard X-rays arise in a third heavily-obscured magnetically-active component lying very close to FU Ori. This component could be related to the hotspot detected in the interferometer observations of Malbet et al. (2005), or perhaps an object embedded in the disk of FU Ori. It has been suggested that the periodic H $\alpha$  emission of FU Ori might be induced by a low-mass protostar or protoplanet in the disk (Vittone & Errico 2005).

Binarity might at first glance seem to provide an attractive explanation for the unusual double-absorption spectrum of FU Ori. But, the binary hypothesis is not a panacea. Work in progress indicates that the cTTS GV Tau A also has a double-absorption X-ray spectrum, but a *Chandra* observation shows that a known protostellar companion does not contribute to the X-ray emission (Güdel et al., in preparation). Unless an additional companion is present much closer to the star, these results suggest that other factors besides binarity will be needed to fully explain the double absorption spectra.

#### 4.5. Comments on Nonthermal X-ray Emission

The improvement in the fit to the hard component of the FU Ori spectrum that results from replacing the optically thin plasma model with a power-law + Gaussian Fe K line model is substantial (Table 1). This result is somewhat surprising, but some caution is warranted since it is based on the analysis of a relatively low signal-to-noise CCD spectrum.

Although hard power-law X-ray continua are often seen in strongly-accreting compact objects, there is little observational support to date for power-law X-ray emission from magnetically active late-type stars (Güdel 2004). A possible exception is AB Dor, for which a nonthermal X-ray continuum excess was postulated to explain a weak Fe K line in the presence of X-ray flares (Vilhu et al. 1993).

However, the situation encountered for FU Ori is different than for AB Dor. There is no evidence for strong X-ray flaring in the FU Ori light curve and the Fe K emission line is unusually strong, rather than weak. It is thus difficult to argue that any existing power-law emission is related to large X-ray flares. As mentioned above (Sec. 4.3.1), a previous *VLA* radio observation failed to detect FU Ori at 3.6 cm down to rather low limits. Thus, we have no radio evidence for the existence of a population of nonthermal particles in the magnetosphere. Even so, additional centimeter radio observations at longer wavelengths might be worthwhile since nonthermal radio flux density typically increases with wavelength.

If a power-law component is present, then magnetic accretion might provide an alternative explanation. Lamzin (1999) has discussed the possibility of nonthermal X-ray emission

in accreting PMS stars. If the density of the infalling gas drops below  $n \approx 10^{11} \text{ cm}^{-3}$ , then protons can gyrate many times around a magnetic field line before a collision, and the accretion shock passes into the collisionless regime. In that case, the particle distribution is non-Maxwellian and excess hard X-ray emission can be produced.

At present, the absence of strong X-ray flares and the lack of a radio detection of FU Ori, along with the strong Fe K line, suggest that the X-ray emission is predominantly thermal. A higher signal-to-noise spectrum will be needed to distinguish between purely thermal models and models that invoke a hard power-law continuum.

## 5. Summary

The double-absorption X-ray spectrum of FU Ori is unusual compared to most TTS, but in some respects does resemble that of the jet-driving cTTS DG Tau A (Güdel et al. 2005). However, there are also notable differences. The spectrum of DG Tau A does not show a strong Fe K line as is present in FU Ori, and there is no evidence to date that FU Ori has a jet-like outflow. If the cool low-absorption X-ray emission detected in DG Tau A is related to a shocked jet (Güdel et al. 2005) then it is not obvious that this interpretation applies to FU Ori as well.

In general, the existing data give little reason to invoke shock-induced X-rays to explain the emission in the FU Ori spectrum, despite the belief that it is accreting at high rates. Clearly, higher angular resolution observations would be useful to determine if the soft emission is slightly offset from the star, as might be the case if it originates in a shocked jet or outflow. A higher angular resolution *Chandra* observation might also shed light on whether the faint near-IR companion located  $0.5''$  south of FU Ori contributes to the X-ray emission.

The overall temperature structure of the FU Ori spectrum strongly resembles that seen in active late-type coronal sources, including magnetically-active PMS stars. Thus, a coronal origin seems likely, at least for the hot plasma component. Assuming that the emission is coronal, then the nature and location of the material responsible for the strong absorption of the hard X-ray component remains the most intriguing question. Either cold accreting gas or a strong neutral wind are the most likely candidates, but an inhomogeneous absorber or non-spherical geometries are needed if both the cool and hot plasma originate close to the star.

Even though FU Ori is the prototype, it would be premature to conclude that its unusual X-ray properties are representative of the class of FUors as a whole. Prototypes can show extreme or unusual behavior and T Tauri itself is a well-known example. Additional

observations of other FUors are needed to define the X-ray properties of the class and such observations are now pending.

This research was supported by NASA grants NNG04GH23G and NNG05GJ15G. Work at PSI (MG) was supported by the Swiss National Science Foundation, grant number 20-66875.01. This work is based on observations obtained with *XMM-Newton*, an ESA science mission with instruments and contributions directly funded by ESA member states and the USA (NASA).

## REFERENCES

- Adams, F.C., Lada, C.J., & Shu, F.H., 1987, ApJ, 312, 788
- Anders, E., & Grevesse, N. 1989, Geochim. Cosmochim. Acta, 53, 197
- Calvet, N., Hartmann, L., & Kenyon, S.J., 1993, ApJ, 402, 623
- Clarke, C., Lodato, G., Melnikov, S.Y., & Ibrahimov, M.A., 2005, MNRAS, 361, 942
- Croswell, K., Hartmann, L., & Avrett, E.H., 1987, ApJ, 312, 227
- Drake, J.J., 2005, in *Cool Stars, Stellar Systems, and the Sun (13th Cambridge Workshop)*, eds. F. Favata et al. (ESA), in press.
- Getman, K.V. et al., 2005, ApJS, 160, 319
- Gorenstein, P., 1975, ApJ, 198, 95
- Güdel, M., 2004, A&A Rev., 12, 71
- Güdel, M., Skinner, S.L., Briggs, K.R., Audard, M., Arzner, K., & Telleschi, A., 2005, ApJ, 626, L53
- Hartmann, L. & Kenyon, S.J. 1996, ARA&A, 34, 207 (HK96)
- Herbig, G.H. 1966, Vistas in Astron., 8, 109
- Herbig, G.H. 1977, ApJ, 217, 693
- Herbig, G.H., Petrov, P.P., & Duemmler, R., 2003, ApJ, 595, 384
- Kastner, J.H., Huenemoerder, D.P., Schulz, N.S., Canizares, C.R., & Weintraub, D.A., 2002, ApJ, 567, 434



- Kenyon, S.J., Hartmann, L., & Hewett, R., 1988, ApJ, 325, 231
- Lamzin, S.A., 1999, Astron. Letters, 25, 430
- Levreault, R.M., 1988, ApJ, 330, 897
- Malbet, F. et al. 2005, A&A, 437, 627
- Petrov, P.P. & Herbig, G.H., 1992, ApJ, 392, 209
- Preibisch, T. & Feigelson, E.D., 2005, ApJS, 160, 390
- Raga, A.C., Noriega-Crespo, A., & Velázquez, P.F., 2002, ApJ, 576, L149
- Reipurth, B. & Aspin, C. 2004, ApJ, 608, L65
- Rodriguez, L.F., Hartmann, L.W., & Chavira, E., 1990, PASP, 102, 1413
- Sandell, G. & Weintraub, D.A. 2001, ApJS, 134, 115
- Schmitt, J.H.M.M., Robrade, J., Ness, J.-U., Favata, F., & Stelzer, B., 2005, A&A, 432, L35
- Skinner, S.L., Brown, A., & Stewart, R.T., 1993, ApJS, 87, 217
- Skinner, S., Güdel, M., Briggs, K., Melnikov, S., & Audard, M., 2005, Ap&SS (Conf. Proceed. *Close Binaries in the 21st Century: New Opportunities and Challenges*), eds. A. Gimenez, E. Guinan, P. Niarchos & S. Rucinski, in press
- Smith, H.A., Thronson, H.A., Lada, C.J., Harper, D.A., Loewenstein, R.F., & Smith, J., 1982, ApJ, 258, 170
- Strüder, L. et al. 2001, A&A, 365, L18
- Turner, M.J.L. et al. 2001, A&A, 365, L27
- Ulrich, R.K. 1976, ApJ, 210, 377
- Usov, V.V. & Melrose, D.B., 1992, ApJ, 395, 575
- Vilhu, O. et al., 1993, A&A, 278, 467
- Vittone, A.A. & Errico, L., 2005, Mem. S.A. It., 76, 320
- Wang, H., Apai, D., Henning, T., & Pascucci, I., 2004, ApJ, 601, L83

Table 1. *XMM-Newton* Spectral Fits for FU Ori

Parameter				
Model <sup>a</sup>	A	B	C	D
Emission	thermal	thermal	thermal	thermal + power-law + line
Abundances	solar	Fe varied	Fe varied	solar
$N_{H,1}$ ( $10^{22}$ cm $^{-2}$ )	0.55 [0.02 - 1.13]	0.42 [0.00 - 1.81]	0.35 [0.12 - 0.90]	0.35 [0.23 - 1.11]
$kT_1$ (keV)	0.65 [0.17 - 0.86]	0.67 [0.08 - 1.01]	0.68 [0.14 - 1.04]	0.69 [0.08 - 1.03]
$norm_1$ ( $10^{-6}$ ) <sup>b</sup>	6.22 [1.76 - .....]	4.68 [0.49 - 27.1]	4.87 [0.36 - .....] <sup>d</sup>	3.30 [0.90 - 8.52]
$N_{H,2}$ ( $10^{22}$ cm $^{-2}$ )	12.8 [8.25 - 20.2]	8.44 [5.58 - 13.7]	10.6 [6.76 - 18.6]	4.38 [1.62 - 8.76]
$kT_2$ (keV)	5.58 [3.99 - 9.01]	7.17 [4.90 - 10.2]	7.04 [4.86 - 10.3]	...
$norm_2$ ( $10^{-5}$ ) <sup>b</sup>	18.4 [12.2 - 27.2]	10.6 [6.70 - 16.4]	29.8 [12.5 - 50.6] <sup>e</sup>	0.62 [0.31 - 1.99]
$\Gamma$	...	...	...	0.72 [0.07 - 1.61]
$E_{line}$ (keV)	...	...	...	6.68 [6.56 - 6.75]
$\sigma_{line}$ (keV)	...	...	...	0.10 [0.06 - 0.25] <sup>g</sup>
$norm_{line}$ ( $10^{-6}$ )	...	...	...	2.58 [1.60 - 3.86]
Fe <sub>1</sub>	{1.0}	0.87 [0.00 - .....] <sup>c,f</sup>	{1.0}	{1.0}
Fe <sub>2</sub>	{1.0}	$\geq 1.0$ <sup>c,f</sup>	2.52 [1.24 - 4.83]	...
$\chi^2/dof$	27.3/26	21.6/24	21.0/24	13.6/24
$\chi^2_{red}$	1.05	0.90	0.88	0.56
$F_X$ ( $10^{-14}$ ergs cm $^{-2}$ s $^{-1}$ )	7.93 (31.3)	8.57 (21.9)	8.58 (68.7)	8.49 (12.6)
$F_{X,1}$ ( $10^{-14}$ ergs cm $^{-2}$ s $^{-1}$ )	0.37 (1.58)	0.34 (1.06)	0.58 (1.11)	0.31 (0.82)
$F_{X,line}$ ( $10^{-14}$ ergs cm $^{-2}$ s $^{-1}$ )	1.40 (1.69)	2.05 (2.32)	1.95 (2.28)	2.33 (2.48)
$L_X$ ( $10^{30}$ ergs s $^{-1}$ )	7.91	5.55	17.4	2.99
$\log [L_X/L_{bol}]$	-5.23	-5.38	-4.89	-5.65

Note. — Based on XSPEC (vers. 12.2.0) fits of the background-subtracted EPIC PN spectrum binned to a minimum of 10 counts per bin using 26.9 ksec of low-background exposure. Thermal emission was modeled with the *vapex* optically thin plasma model in XSPEC. The tabulated parameters are absorption column density ( $N_H$ ), plasma energy ( $kT$ ), component normalization ( $norm$ ), photon power-law index ( $\Gamma$ ), Gaussian line centroid energy ( $E_{line}$ ), line width ( $\sigma_{line} = FWHM/2.35$ ), and Fe abundance relative to the solar photospheric value. Solar abundances are referenced to Anders & Grevesse (1989). Square brackets enclose 90% confidence intervals and an ellipsis means that the algorithm used to compute confidence intervals did not converge. Curly braces {...} enclose quantities that were held fixed during fitting. The total X-ray flux ( $F_X$ ) and flux of the low-absorption component ( $F_{X,1}$ ) are the absorbed values in the 0.5 - 7 keV range, followed in parentheses by unabsorbed values. The continuum-subtracted Fe K line flux ( $F_{X,line}$ ) is measured in the 6.5 - 6.84 keV range. The unabsorbed luminosity  $L_X$  (0.5 - 7 keV) assumes a distance of 460 pc. A value  $L_{bol} = 350 L_\odot$  is adopted based on an average of values given in the literature (HK96, Levreault 1988, Sandell & Weintraub 2001, Smith et al. 1982).

<sup>a</sup>Model A and B:  $N_{H,1} \cdot kT_1 + N_{H,2} \cdot kT_2$ ; Model C:  $N_{H,1} \cdot (kT_1 + kT_2) + N_{H,2} \cdot (kT_1 + kT_2)$ ; Model D:  $N_{H,1} \cdot kT_1 + N_{H,2} \cdot (PL + GAUSS)$

<sup>b</sup>For thermal *vapex* models, the  $norm$  is related to the emission measure (EM) by  $EM = 4\pi 10^{14} d_{cm}^2 \times norm$ , where  $d_{cm}$  is the stellar distance in cm.

<sup>c</sup>The Fe abundance of the cool plasma component (Fe<sub>1</sub>) is not well-constrained by the data. The derived iron abundance of the hot plasma component (Fe<sub>2</sub>) is largely determined by the fit to the Fe K emission line and is moderately sensitive to the amount of spectral binning. When binned to a minimum of 10 counts per bin the derived value is  $Fe_2 = 2.78$  [1.40 - 5.29; 90% conf.]  $\times$  solar. At a minimum of 15 counts per bin the derived value is  $Fe_2 = 2.20$  [0.98 - 4.19].

<sup>d</sup>The quoted value  $norm_1$  is the total normalization factor for the low-absorption component, which is the sum of the norms for cool and hot plasma:  $norm_1 = norm_{1,cool} + norm_{1,hot}$ . The best-fit gives  $norm_{1,cool}/norm_{1,hot} = 1.59$

<sup>e</sup>The quoted value  $norm_2$  is the total normalization factor for the high-absorption component:  $norm_2 = norm_{2,cool} +$

$\text{norm}_{2,hot}$ . The value of  $\text{norm}_{2,cool}$  is constrained during the fit to  $\text{norm}_{2,cool} = [\text{norm}_{1,cool}/\text{norm}_{1,hot}] \times \text{norm}_{2,hot}$ .

<sup>f</sup>If the global metallicity  $Z$  is allowed to vary instead of just Fe alone, then the best fit  $N_H$  and  $kT$  values change by less than 7%. The best-fit metallicities are  $Z_1 = 0.99$  [0.01 - 1.61] and  $Z_2 = 3.56$  [1.04 - 5.00].

<sup>g</sup>If a second Gaussian component is added at  $E_{line} = 6.36$  keV to model the weak excess that may be due to Fe I, then the width of the Fe K line converges to a value  $\sigma_{line} = 0.063$  [0.00 - 0.20] keV that is consistent with no excess broadening beyond instrumental.

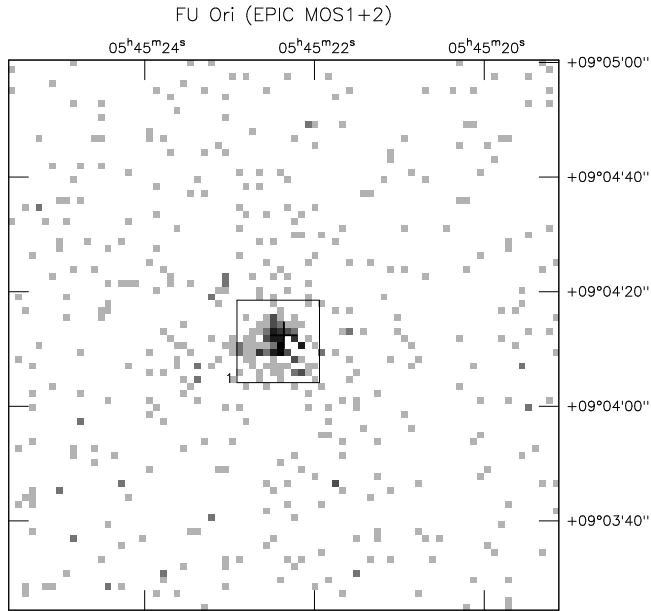


Fig. 1.— Combined EPIC MOS1 + MOS2 image of FU Ori (172 net counts, 32.2 ksec per MOS) in the 0.5-7 keV range. Cross marks 2MASS position of FU Ori. Pixel size is  $1.1''$  and coordinates are J2000.

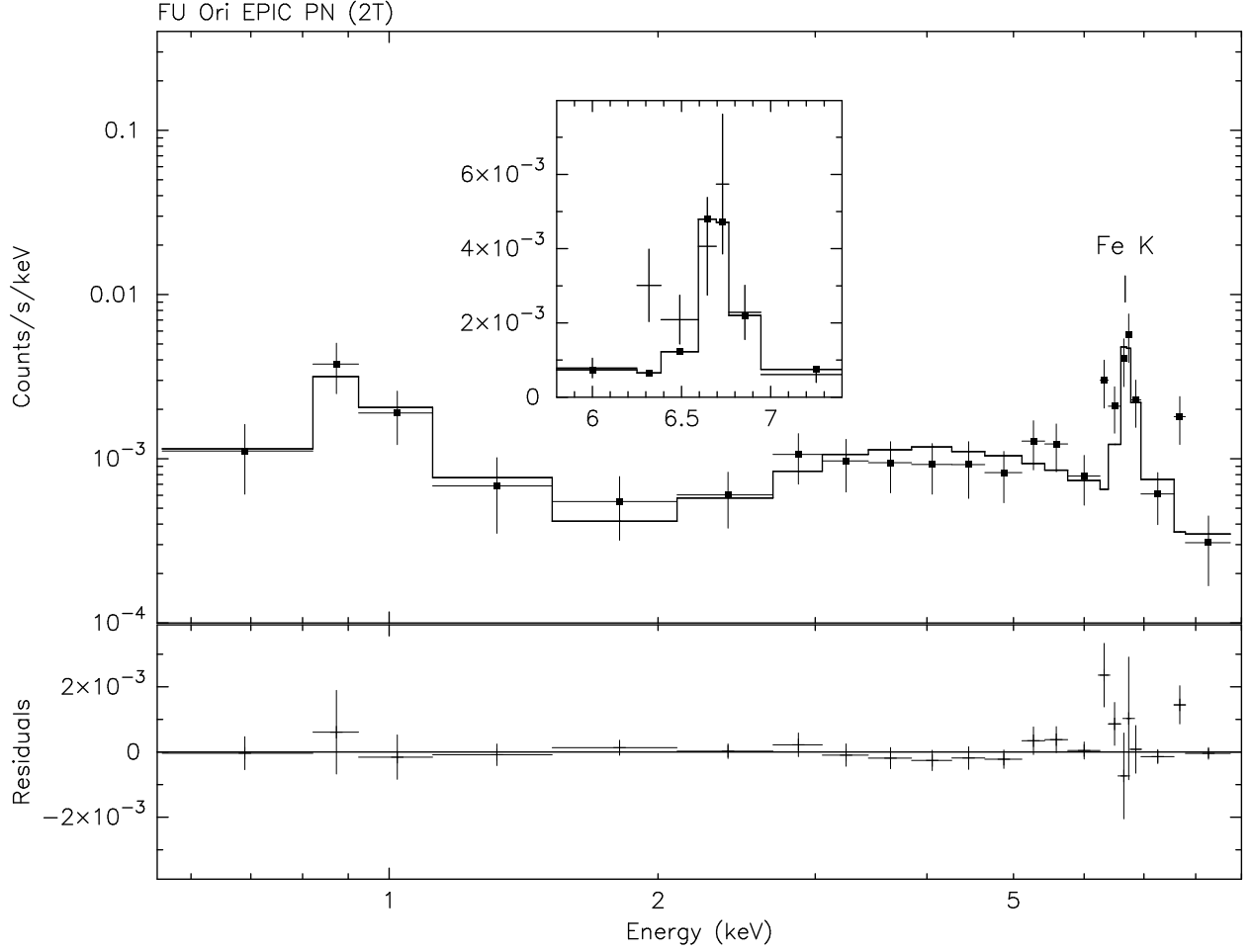


Fig. 2.— Background subtracted EPIC PN spectrum of FU Ori obtained on 2005 Apr 3-4 using 26891 s of low-background exposure ( $\approx 200$  net counts in the 0.5 - 7 keV range). The spectrum (filled squares) is binned to a minimum of 10 counts per bin. The overlaid model (solid line) is a double-absorption model with two thermal plasma components and variable Fe abundance (Model B in Table 1). The Fe K line fit includes only instrumental broadening. The inset shows the fit to the Fe K line on a linear axis scale.

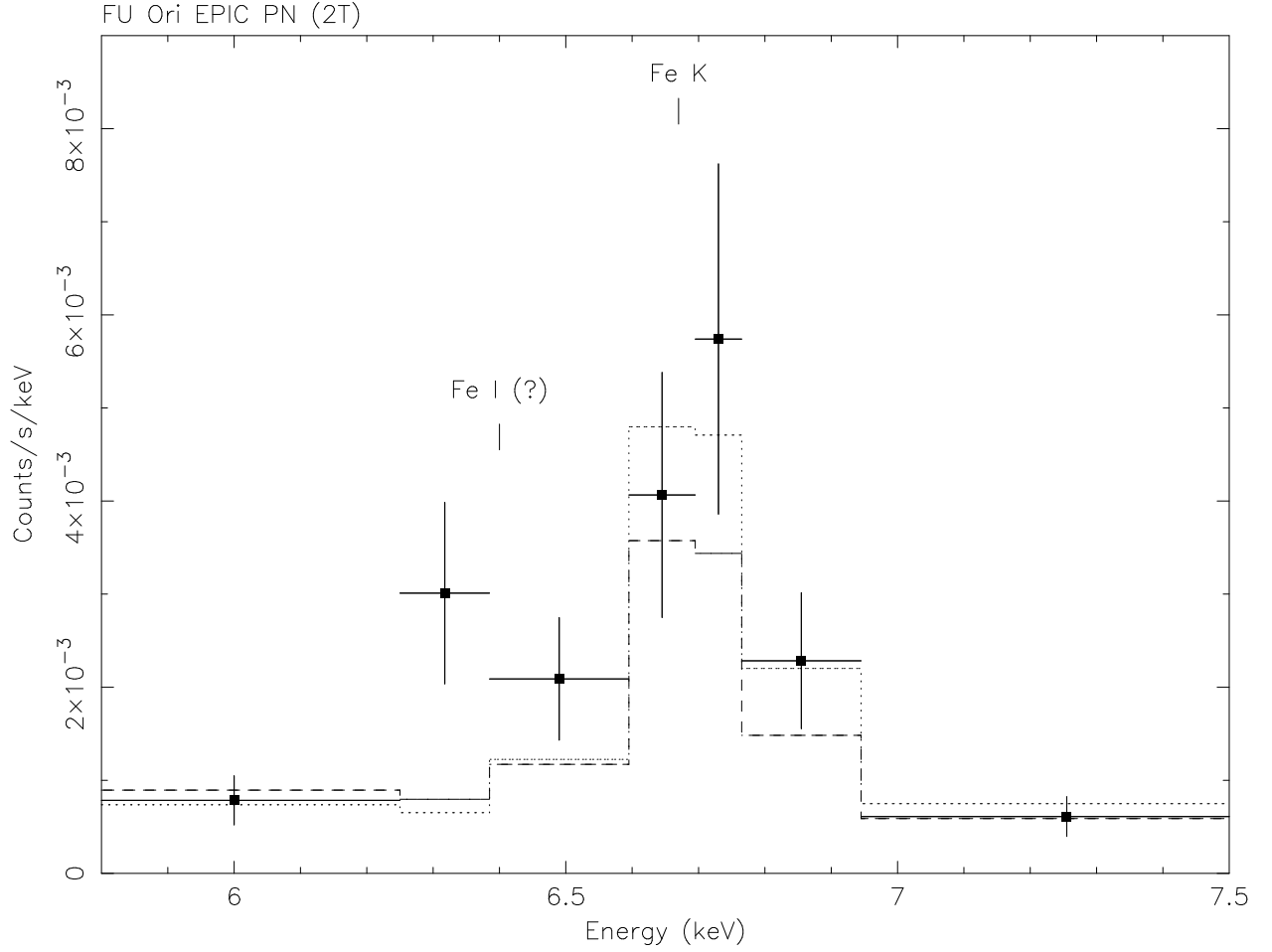


Fig. 3.— Fits of the Fe K line in the EPIC PN spectrum of FU Ori with a double-absorption thermal plasma model. The dashed line shows the best-fit using solar abundances (Model A in Table 1) and the dotted line shows the best-fit when the Fe abundances are allowed to vary (Model B.). The excess emission near 6.4 keV may be due to fluorescent Fe I.

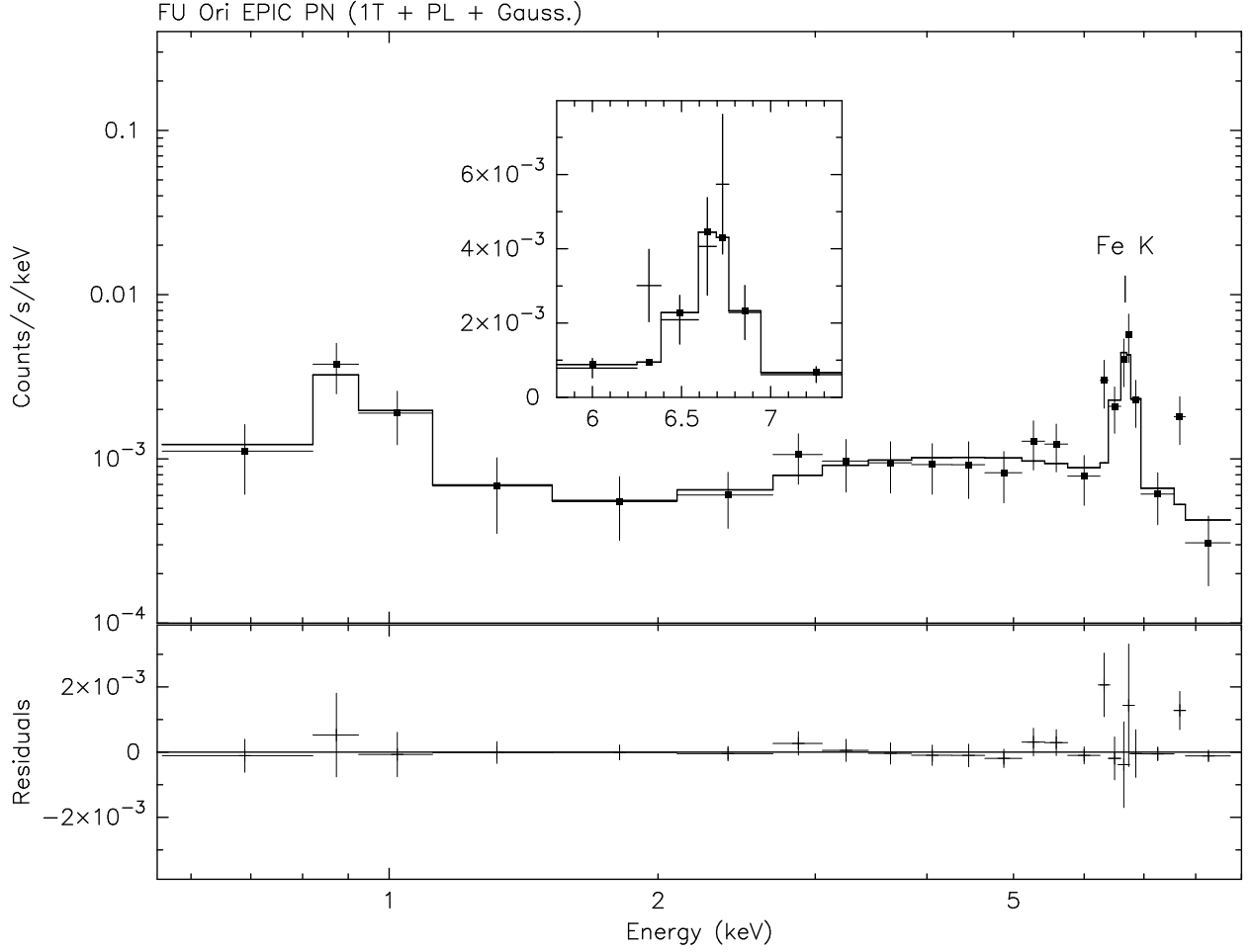


Fig. 4.— Same as Fig. 2 except the overlaid model is 1T + PL + Gaussian Fe K line (Model D in Table 1). The Gaussian line width was allowed to vary to achieve a best-fit. The inset shows the fit in the vicinity of the Fe K line on a linear axis scale. The fit attempts to account for some of the excess below 6.5 keV and thus slightly overestimates the true Fe K line width.